New Developments in Clathrate Research

Michael Baitinger, Lev Akselrud[1], Umut Aydemir, Matt Beekman[2], Bodo Böhme, Horst Borrmann, Ulrich Burkhardt, Christophe Candolfi, Wilder Carrillo-Cabrera, Katherine Chiong[3], Arnold Guloy[3], Ying Liang, Hannes Lichte[4], Katrin Meier, Hong Duong Nguyen, George Nolas[2], Niels Oeschler, Yurii Prots, Marianne Reibold[4], Marcus Schmidt, Walter Schnelle, Ulrich Schwarz, Paul Simon, Zhongjia Tang[3], Igor Veremchuk, Aron Wosylus, Hui Zhang, Jing-Tai Zhao[5], Frank Steglich and Yuri Grin

Intermetallic clathrates have continued to be an essential joint project at the institute. During the recent research period long-standing questions were elucidated, and new perspectives in the field were opened. Despite intense research activities on intermetallic clathrates, fundamentally new results can still be achieved by applying advanced experimental methods and the concerted research action of chemists and physicists.

$BaGe_5$: A new Type of Intermetallic Clathrates

The great majority of intermetallic clathrate phases form crystal structures related to type I and type II gas hydrates. These phases are characterized by covalently-bonded host frameworks of, typically, group-14-elements encapsulating electropositive metal atoms. However, with increasing content of electropositive elements connectivity patterns become more complex. A well-known example is the chiral clathrate type with Pearson symbol *cP*124, in which metal-centered pentagonal dodecahedral cages enclose a zeolite-type labyrinth containing chains of the remaining metal atoms [1]. The new crystal structure type of $BaGe_5$ (*oP*60, space group *Pmna*) [2] may be described as an intermediate between $Ba_8Ge_{43}\square_3$ (*cP*54-3) [3] and Ba_6Ge_{25} (*cP*124) [4]. The crystal structure of $BaGe_5$ reveals only one type of polyhedron, Ge_{20} pentagonal dodecahedra, which are centered by Ba atoms. The remaining Ba atoms are either assembled in channels as in Ba_6Ge_{25} or located in cavities which are similar to the Ge_{24} cages in $Ba_8Ge_{43}\square_3$ (Fig. 1). The Ge_{20} polyhedra are arranged via common pentagons and hexagons to 2D layers perpendicular to [010]. These 2D layers are covalently interconnected via disordered $(3b)Ge^-$ species which alternatively occupy two neighboring positions. The electronic balance expressed by $[Ba^{2+}][(3b)Ge^-]_2[(4b)Ge^0]_3$ fulfills the counting scheme of a Zintl phase.

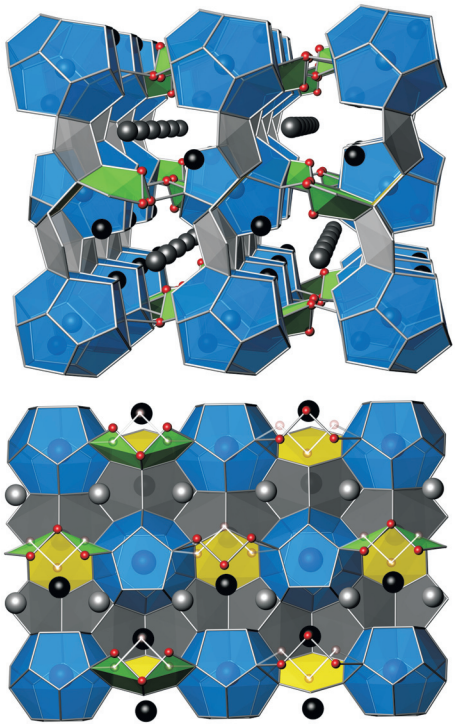

Fig. 1: Crystal structure of $BaGe_5$ with channels and covalently bonded layers along [100] (top); view down [010] (bottom). Ba atoms are represented by large spheres in black and grey, the disordered Ge sites are drawn in red and white.

$BaGe_5$ decomposes at around 820 K in a peritectoid reaction to Ba_6Ge_{25} and α-Ge. The reverse reaction is kinetically hindered which is probably the reason why the phase was not identified in thermodynamic equilibrium before. We succeeded in the preparation of $BaGe_5$ by disproportionation of the high-temperature-phase $Ba_8Ge_{43}\square_3$. Hence, microcrystalline products contained ≈ 5 wt-% of α-Ge. As a consequence of this discovery of a new equilibrium phase in the system Ba–Ge, the phase relations of the various multinary thermoelectric clathrates based thereon should be reconsidered. The clathrate $BaGe_5$ constitutes a diamagnetic semiconductor and hence may represent a new prototype structure for thermoelectric materials.

$Cs_{8-x}Si_{46}$ and $Cs_{8-x}Ge_{44+y}$: New type-I Clathrates

Until recently, a binary clathrate-I phase with Cs had only been known for tin [5]. Although clathrate frameworks can adapt to various kinds of filler atoms, Cs was believed to be too large to be accommodated in Si and Ge frameworks. Surprisingly, the new binary clathrates were obtained by high-pressure syntheses [6, 7]. Both phases do not only show large interatomic distances *d*(Ge–Ge) and *d*(Si–Si), but also exhibit the largest lattice parameters ever observed for binary silicon and germanium type-I clathrates, respectively. The existence of clathrate phases with expanded unit cell volume at high pressure may be unexpected but the overall volume decreases upon clathrate formation if compared to the respective educts. For instance, the volume change for a reaction such as 2 Cs_4Ge_9 + 26.4 Ge → $Cs_8Ge_{44.40(2)}\square_{1.60(2)}$ is calculated to be about –273 Å^3 per formula unit considering cell parameters at ambient pressure. Hence, the formation of the clathrate-I is supported by the application of pressure, as it was similarly observed for $Ba_{8-x}Si_{46}$ [8]. For both $Cs_{8-x}Si_{46}$ and $Cs_{8-x}Ge_{44+y}$ the reaction conditions have a strong influence on the composition. For the silicon clathrate, the occupation of the smaller Si_{20} cages by Cs atoms increased with pressure, while the Cs positions in the larger Si_{24} cages and the Si framework sites were always fully occupied. According to X-ray powder diffraction data the composition ranged from $Cs_{6.9}Si_{46}$ (≈ 2 GPa, ≈ 1200 K) to $Cs_{7.8}Si_{46}$ (≈ 10 GPa, ≈ 1200 K). In contrast to the $Cs_{8-x}Si_{46}$ phase, the germanium clathrate contains vacancies in the framework (Fig. 2) as it was similarly observed for $K_8Ge_{44}\square_2$ or $Cs_8Sn_{44}\square_2$. However, structure refinement of single crystal X-ray diffraction data revealed the chemical composition $Cs_8Ge_{44.40(2)}\square_{1.60(2)}$. The higher Ge content is surprising, because 2 vacancies □ per formula unit are expected for an ideal Zintl phase with charge-balanced composition, according to $[Cs^+]_8[(3b)Ge^-]_8[(4b)Ge^0]_{36}$. The structure analysis reveals a reduced free volume in the Ge_{24} cage due to vacancy formation, which would be unfavorable for a large filler atom [7]. However, only neutral Cs atoms would be too large for the cages considering atomic radii. This might indicate that the Cs atoms do not fully transfer their valence electron to the Ge framework.

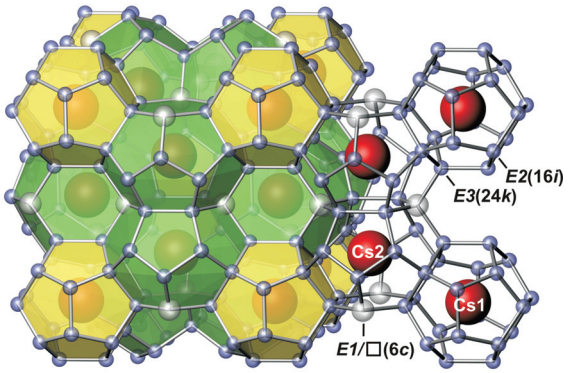

Fig. 2: Crystal structure of the clathrate-I $Cs_{8-x}Ge_{44+y}\square_{2-y}$. with defect positions in the Ge framework [8]. Cs atoms are drawn in red, the partially occupied Ge site is represented by transparent spheres, the fully occupied Ge sites by blue spheres.

Synthesis of Clathrates by Redox Reactions

The preparation of the allotrope Ge (*cF*136) by oxidation of $Na_{12}Ge_{17}$ with an ionic liquid has opened up new perspectives for the preparation of intermetallic phases at low temperatures [9]. Meanwhile, the purity of the bulk products has been distinctly enhanced by utilising of gas-solid-reactions [10] (see contribution *The Role of Ionic Liquids in the Preparation of Intermetallic Clathrates and Related Element Modifications*). The method was successfully applied to the synthesis of $Ba_{8-x}Si_{46}$ [11], which has attracted particular interest as superconductor with silicon framework [12]. The preparation at ambient pressure and low reaction temperatures is remarkable because this phase could, so far, only be prepared by high-pressure, high-temperature syntheses [8]. However, the existence field of $Ba_{8-x}Si_{46}$ is not fully understood. Calculation of ground-state energies for $BaSi_2$, α-Si and Ba_8Si_{46} indicates that the clathrate with fully occupied Ba sites is stable only at high pressure [13]. On the other hand, a high-pressure product with composition $Ba_{7.76}Si_{46}$ was transformed by annealing at 800 K and under vacuum to a clathrate with lower Ba content, namely $Ba_{6.63}Si_{46}$ [14]. From the latter result it might be concluded that, for lower Ba content, the clathrate phase is stable at ambient pressure in this temperature range. The preparation of $Na_2Ba_6Si_{46}$ [15] by oxidation of Na_2BaSi_4 led us then to the question of whether $Ba_{8-x}Si_{46}$ can also be prepared at ambient pressure by this method. However, our first experiments to oxidize the precursor phases Ba_3Si_4 or $BaSi_2$ with gaseous HCl

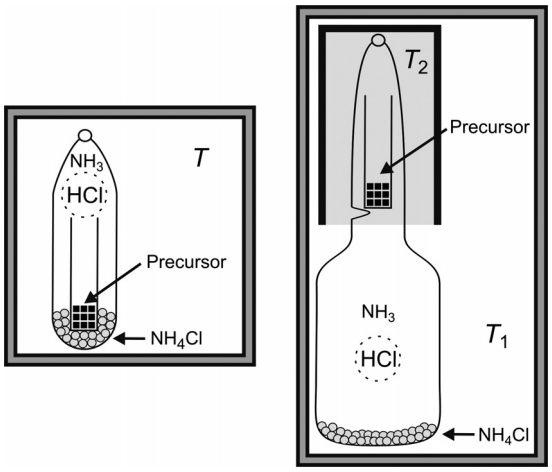

Fig. 3: Setup for the oxidation of intermetallic compounds with HCl [11]: (left) the precursor and NH_4Cl are placed spatially separated at the same temperature T; (right) using a two-zone furnace, the precursor is placed in the high-temperature zone (T_2), while NH_4Cl is placed in the low-temperature zone of the ampoule (T_1).

resulted in the formation of nano-porous silicon [16, 17]. The reaction had been performed in a closed ampoule in which the precursor and NH_4Cl were placed spatially separated (Fig. 3, left). In this setup, gaseous HCl is generated from NH_4Cl upon heating. In order to control the oxidation reaction, a low partial pressure of HCl is required such that only low reaction temperatures of about 573 K should be applied. By using an improved experimental setup with two different temperature zones (Fig. 3, right) the reaction temperature of the precursor and the partial pressure of HCl could be independently adjusted. This way, polycrystalline samples of $Ba_{8-x}Si_{46}$ could be prepared by oxidation of Ba_3Si_4 and $BaSi_2$ [17].

The yield and crystallinity of the clathrate phase could be substantially enhanced by using $Ba_4Li_2Si_6$ as an alternative precursor. This is attributed to the high mobility of Li during the redox process in which the crystal structure of the solid substrate is rearranged [11]. While Li reacts to LiCl, it was not detected in the clathrate product anymore. Using $Ba_4Li_2Si_6$ it is possible to achieve the clathrate product within only a few minutes of reaction time. Depending on the reaction conditions, the clathrate phase could be obtained in high yield with compositions ranging from $Ba_{6.18(1)}Si_{46}$ to $Ba_{6.62(2)}Si_{46}$. Our preparation route provides an alternative to the high-pressure route and may provide access to bulk products of $Ba_{8-x}Si_{46}$.

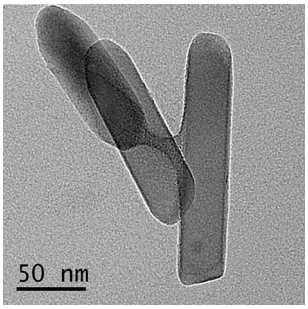

Fig. 4: TEM image of rod-shaped clathrate-II K_xGe_{136} nanoparticles obtained by oxidation of K_4Ge_9 [19].

This example shows that the preparation of crystalline reaction products by the oxidation method requires elaborate adjustment of the reaction conditions, while X-ray amorphous products are easily obtained. However, this fact has been exploited to prepare interesting nano-structured products [18]. Crystalline nano-sized particles of the clathrate-II phases K_xGe_{136} and Na_xSi_{136} are obtained from a dispersion of alkali metal tetrelides in an ionic liquid [19]. The morphology of the nanoparticles is revealed by means of electron holography and high-resolution electron microscopy. The particles are typically bullet-shaped with dimensions of 15 nm – 60 nm in width and 100 nm – 300 nm in length (Fig. 4). The preparation route might facilitate the access to silicon- and germanium-based crystalline nanostructures.

$Na_{24}Si_{136}$: Preparation and Crystal Growth

For the first time, spark plasma sintering (SPS) was successfully employed as a route for the synthesis and crystal growth of intermetallic clathrates [20]. The method represents an electrochemical variant of the redox reactions of precursor phases. A single-phase product of $Na_{24}Si_{136}$ was obtained containing single crystals of up to 500 µm in size (Fig. 5). This is remarkable as binary silicon clathrates are usually formed as microcrystalline products by any other preparation method. Historically, $Na_{24-x}Si_{136}$ was the first structurally identified clathrate-II phase [21]. It has been obtained with Na deficiency only, and with clathrate-I or α-Si as impurity phases directly by thermal decomposition of Na_4Si_4. Single crystals of $Na_{24}Si_{136}$ were obtained by SPS treatment of Na_4Si_4 at 873 K for 3 hours, under uniaxial pres-

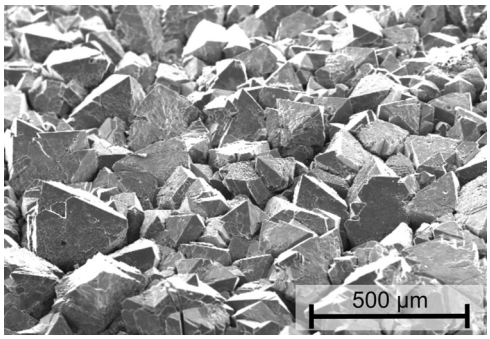

Fig. 5: Scanning electron microscope image of $Na_{24}Si_{136}$ crystals obtained after SPS treatment of Na_4Si_4 at 600 °C.

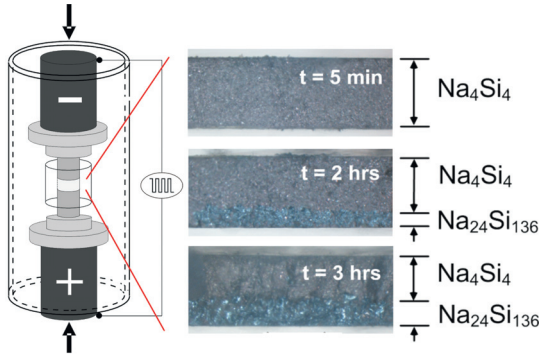

Fig. 6: SPS preparation of $Na_{24}Si_{136}$: (left) reaction tool; (right) cross sections of specimens treated by SPS at 600 °C and 100 MPa. The formation of $Na_{24}Si_{136}$ from Na_4Si_4 in dependence on the reaction time is cleary visible.

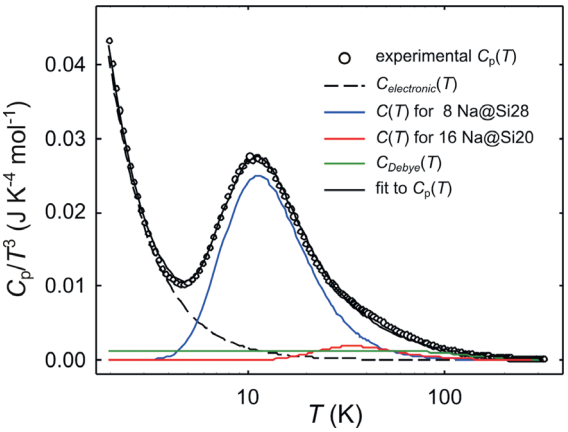

Fig. 7: Experimental (dots) and calculated (black line) heat capacity of $Na_{24}Si_{136}$ plotted as C_p/T^3. The dashed line represents the electronic contributions, red and blue lines the individual contributions of the Na atoms applying the Einstein model [23].

sure of 100 MPa. The specimen was subjected to ms-pulsed DC electrical current, with the punches serving as electrodes (Fig. 6). The whole setup was situated inside an argon-filled glove box for protection against oxidation and moisture [22].

After the spark plasma treatment, a thin film of Na is always found condensed at the cathode while the clathrate formation started at the anode progressing towards the cathode (Fig. 6). By changing the direction of current, the clathrate phase grows in the inverse direction, which unambiguously proves the influence of the DC electrical current on the reaction. $Na_{24}Si_{136}$ forms by oxidation of Si_4^{4-} at the anode, whereas sodium is reduced at the cathode. Upon oxidation of the Si_4^{4-} cluster anions, the clathrate framework is formed, while sodium is simultaneously encapsulated in the resulting Si_{20} and Si_{28} cages. The crystal structure of the $Na_{24}Si_{136}$ was investigated in detail. A very large atomic displacement parameter is observed for Na atoms centered in the Si_{28} cage. A difference Fourier map calculated with Na removed from the model shows only a broadly smeared, essentially spherical residual density, with a clear maximum at the center of the cage reflecting a thermal motion ('rattling'). This is corroborated by Einstein-like modes attributed to Na atom "rattling" which was observed to provide a pronounced contribution to the heat capacity [23] (Fig. 7). The importance of the new preparation method can be seen from the fact that it has been highly challenging to prepare dense specimens of silicon clathrates free from detrimental grain boundary effects.

$Ba_8Au_{5.3}Ge_{40.7}$: A *p*-type Clathrate-I with high thermoelectric Efficiency

The clathrate phase in the system Ba–Au–Ge was initially assigned to the composition $Ba_8Au_6Ge_{40}$ [24]. A material of this composition shows bad-metal behavior [25]. In fact, the clathrate phase exhibits a wide phase range with promising thermoelectric properties. To provide a reliable basis for physical property measurements a single crystalline specimen was prepared as reference material by using the Bridgman technique [26]. The crystal exhibits *p*-type electrical conductivity, low thermal conductivity and a high Seebeck coefficient. The maximum thermoelectric figure of merit was found to be ZT = 0.3 at 511 K. SPS-compacted finely ground samples with a slightly different composition show an increase of ZT up to 0.9 at 680 K, opening up the opportunity for further optimization of thermoelectric properties.

Summary

With $BaGe_5$, a new type of clathrate (*oP*60) was characterized. Based hereupon the phase relations in the system Ba–Ge were revised. Applying high pressure synthesis the preparation of the so far unknown clathrate-I phases $Cs_{8-x}Si_{46}$ and $Cs_{8-x}Ge_{44+y}$ was achieved. The reaction of intermetallic precursors with oxidizing agents has been established as a versatile preparation method. Using gas-solid reactions, the clathrate phase $Ba_{8-x}Si_{46}$ was obtained which, so far, had been accessible under high-pressure conditions only. Liquid solid redox reactions of precursors with an ionic liquid resulted in the formation of nanosized clathrate phases. For the first time, a clathrate phase, $Na_{24}Si_{136}$, was obtained by using an electrochemical redox process: Crystalline samples were formed by spark plasma sintering of Na_4Si_4. The ternary clathrate-I phase in the system Ba-Au-Ge was obtained with compositions showing promising high thermoelectric efficiency.

B. B., I. V. and Yu. G. gratefully acknowledge funding by the European Union and the Free State of Saxony (SAB projects 13853/2379), M. B. and Yu. G. gratefully acknowledge financial support by the Deutsche Forschungsgemeinschaft (SPP 1415).

References

[1] *H. G. von Schnering, A. Zürn, J.-H. Chang, M. Baitinger, and Yu. Grin,* Z. Anorg. Allg. Chem. **633** (2007) 1147.
[2] *U. Aydemir, L. Akselrud, W. Carrillo-Cabrera, C. Candolfi, N. Oeschler, M. Baitinger, F. Steglich, and Yu. Grin,* J. Am. Chem. Soc. **132** (2010) 10984.
[3] *U. Aydemir, C. Candolfi, H. Borrmann, M. Baitinger, A. Ormeci, W. Carrillo-Cabrera, C. Chubilleau, B. Lenoir, A. Dauscher, N. Oeschler, F. Steglich, and Yu. Grin,* Dalton Trans. **39** (2010) 1078.
[4] *W. Carrillo-Cabrera, J. Curda, H. G. von Schnering, S. Paschen, and Yu. Grin,* Z. Kristallogr. **215** (2000) 207.
[5] *H. G. von Schnering, R. Kroener, M. Baitinger, K. Peters, R. Nesper, and Yu. N. Grin*, Z. Kristallogr. NCS **215** (2000) 205–206.
[6] *A. Wosylus, I. Veremchuk, W. Schnelle, M. Baitinger, U. Schwarz, and Yu. Grin,* Chem. Eur. J. **15** (2009) 5901.
[7] *I. Veremchuk, A. Wosylus, B. Böhme, M. Baitinger, H. Borrmann, Yu. Prots, U. Burkhardt, U. Schwarz, and Yu. Grin,* Z. Anorg. Allg. Chem. **637** (2011), 1281.
[8] *S. Yamanaka, H. Fukuoka, E. Enishi, and M. Yasukawa,* Inorg. Chem. **39** (2000) 56.
[9] *A. M. Guloy, R. Ramlau, Z. Tang, W. Schnelle, M. Baitinger, and Yu. Grin,* Nature **443** (2006) 320–323.
[10] *B. Böhme, A. Guloy, Z. Tang, W. Schnelle, U. Burkhardt, M. Baitinger, and Yu. Grin,* J. Am. Chem. Soc. **129** (2007) 5348.
[11] *Y . Liang, B. Böhme, M. Reibold, W. Schnelle, U. Schwarz, M. Baitinger, H. Lichte, and Yu. Grin,* Inorg. Chem. **50** (2011) 4523.
[12] *K. Tanigaki, T. Shimizu, K. M. Itoh, J. Teraoka, Y. Moritomo, and S. Yamanaka,* Nature Materials **2**, (2003) 653.
[13] *Y. Imai and A. Watanabe,* Intermetallics **18** (2010) 542.
[14] *H. Fukuoka, J. Kiyoto, and S. Yamanaka,* Inorg. Chem. **42** (2003) 2933.
[15] *B. Böhme, U. Aydemir, A. Ormeci, W. Schnelle, M. Baitinger, and Yu. Grin,* Sci. Technol. Adv. Mater. **8** (2007) 410.
[16] *U. Aydemir, A. Ormeci, H. Borrmann, B. Böhme, F. Zürcher, B. Uslu, T. Goebel, W. Schnelle, P. Simon, W. Carrillo-Cabrera, F. Haarmann, M. Baitinger, R. Nesper, H. G. von Schnering, and Yu. Grin,* Z. Anorg. Allg. Chem. **634** (2008) 1651.
[17] *B. Böhme,* PhD thesis, TU Dresden, published in Logos Verlag Berlin (2010).
[18] *P. F. McMillan, J. Gryko, C. Bull, R. Arledge, A. J. Kenyon, and B. A. Cressey,* J. Solid State Chem. **178** (2005) 937.
[19] *P. Simon, Z. Tang, W. Carrillo-Cabrera, K. Chiong, B. Böhme, M. Baitinger, H. Lichte, Yu. Grin, and A. M. Guloy,* J. Am. Chem. Soc. **133** (2011) 7596.
[20] *M. Beekman, M. Baitinger, H. Borrmann, W. Schnelle, K. Meier, G. S. Nolas, and Yu. Grin,* J. Am. Chem. Soc. **131** (2009) 9642.
[21] *J. S. Kasper, P. Hagenmuller, M. Pouchard, and C. Cros,* Science **150** (1965) 1713.
[22] *N. Reinfried, P. Höhn, and Yu. Grin,* in Scientific Report 2003-2005, p. 29 (Max Planck Institute for Chemical Physics of Solids, Dresden Germany, 2006).
[23] *M. Beekman, W. Schnelle, H. Borrmann, M. Baitinger, Yu. Grin, and G. S. Nolas,* Phys. Rev. Lett. **104** (2010) 018301.
[24] *G. Cordier and P. Woll,* J. Less Common Met. **169** (1991) 291.
[25] *R. F. W. Herrmann, K. Tanigaki, T. Kawaguchi, S. Kuroshima, and O. Zhou,* Phys. Rev. B **60** (1999) 13245.
[26] *H. Zhang, H. Borrmann, N. Oeschler, C. Candolfi, W. Schnelle, M. Schmidt, U. Burkhardt, M. Baitinger, J.-T. Zhao, and Yu. Grin,* Inorg. Chem. **50** (2011) 1250.

[1] Ivan Franko National University of Lviv, Ukraine
[2] Department of Physics, University of South Florida, Tampa, USA
[3] Department of Chemistry and the Texas Center for Superconductivity, University of Houston, USA
[4] Triebenberg Laboratory, Technical University Dresden
[5] MPG-CAS Partner Group, Key Laboratory of Transparent Opto-Functional Inorganic Materials, Chinese Academy of Science, Shanghai, China